J. Fluid Mech. (2006), *vol.* 559, *pp.* 255–277.
doi:10.1017/S0022112006000267 Printed in the United Kingdom

Space and time organization in a shock-induced separated boundary layer

By P. DUPONT, C. HADDAD AND J. F. DEBIÈVE

Institut Universitaire des Systèmes Thermiques Industriels, Université de Provence and UMR CNRS 6595, 5 rue Enrico Fermi 13, Marseille, Cedex 13, France
pierre.dupont@polytech.univ-mrs.fr

(Received 21 December 2004 and in revised form 20 December 2005)

The interaction of an oblique shock wave impinging on a turbulent boundary layer at Mach number 2.3 is experimentally investigated for a wide range of shock intensities. Characteristic time and length scales of the unsteady reflected shock and inside the downstream interaction region are obtained and compared with already existing results obtained in compression ramp experiments as well as in subsonic detached flows. Dimensionless characteristic frequencies are highlighted to characterize low-frequency shock unsteadiness as well as the different large scales which develop inside the initial part of the interaction. The possibility of describing the spatial development of the large scales inside the interaction zone using a mixing-layer scheme including compressibility effects is tested for a wide range of Mach numbers, shock intensities and geometrical configurations. Moreover, strong evidence of a statistical link between low-frequency shock movements and the downstream interaction is given. Finally, the downstream evolution of the structures shed into the boundary layer is characterized and shows features specific of our configuration.

1. Introduction

The interaction between a shock wave and a turbulent boundary layer is a classical problem found in many supersonic configurations. A simple example, among many other applications, is the design of air intakes or of over-expanded nozzles. The necessity of understanding such flows has motivated numerous experimental, numerical and theoretical studies. Two main configurations have been considered: the compression ramp and the interaction created by an incident shock.

The first one, the compression ramp, has been extensively studied for a wide range of ramp angles and Mach numbers. The main characteristics of this interaction have been obtained (see most classical references in Delery & Marvin (1986) and Smits & Dussauge (1996) and in more recent reviews Dolling (2001), Lee (2001) for example. Experimental results in wind tunnels show that when the shock intensity is strong enough to make the boundary layer separate, the foot of the shock becomes unsteady and oscillates more or less randomly at very low frequencies compared with the characteristic temporal scales of the incoming boundary layer. Moreover, it was shown (Dolling & Murphy 1983; Dolling & Or 1985; Erengil & Dolling 1991*a*) that the unsteadiness of the shock increases with the shock intensity. Some authors tried to correlate the shock oscillations involving low frequencies either with the upstream conditions (Plotkin 1975; Andreopoulos & Muck 1987; Dolling & Brusniak 1989), or with the downstream dynamics of the recirculating zone (Dolling &

Murphy 1983; Dolling & Or 1985; Erengil & Dolling 1991*a*), and obtained much debated conclusions. Thomas, Putman & Chu (1994), tend to conclude that no significant relation could be identified between the upstream boundary layer and the low-frequency shock movement. In contrast, Beresh, Clemens & Dolling (2002), using conditional analysis, showed that some of the low-frequency shock motions could be related to the fullness of the instantaneous velocity profile near the wall of the incoming boundary layer. Another source for the low-frequency shock motions could be the unsteady recirculating zone; however, the precise mechanism is not yet well understood. The main characteristics of the detached zone downstream of the shock wave have been studied (Settles, Vas & Bogdonoff 1976; Ardonceau *et al.* 1980) and present similar behaviour to that of detached subsonic flows: mean velocity profiles strongly modified, high levels of turbulence intensity, turbulence maxima localized far from the wall and a relaxation zone that persists far downstream of the reattachment line. Considering the analysis of Cherry, Hillier & Latour (1984) and Kiya & Sasaki (1983) in subsonic detached flows, some authors suggest describing the initial part of the interaction as a free mixing layer, with the coexistence of two ranges of scales: the first one being associated with the large coherent scales of the mixing layer involving frequencies significantly smaller than in the turbulent initial layer, the second one, one order of magnitude lower, attributed, as in subsonic recirculating flows, to some flapping or pulsation of the flow, the precise nature of this time scale being not well established.

In addition to compression ramps, a second experimental configuration is the reflection of an incident shock wave impinging on the boundary layer. The mean fields, although less well documented than for the compression ramp case, have been obtained for a wide range of configurations (Chapman, Kuehn & Larson 1957; Hakkinen, Greber & Trilling 1959; Green 1970; Delery & Marvin 1986; Deleuze & Elena 1996; Laurent 1996; Garnier & Sagaut 2002). On the other hand, unsteadiness properties are less well documented for this configuration. Nevertheless, similar behaviours to those with the compression ramp have been highlighted such as low-frequency motions of the reflected shock when the shock intensity is strong enough to make the boundary layer separate (Dupont *et al.* 2003, 2004).

In the cases of both the compression ramp and the incident shock wave, when the boundary layer separates, complex phenomena appear with strong unsteadiness involving new time and length scales. Energetic fluctuations are observed in a much lower frequency range than those observed in the incoming turbulent boundary layer. The shock wave turbulent boundary layer interaction (SWTBLI) may result from the superposition or coupling of several elementary problems: low-frequency shock motion, unsteadiness of the separated bubble, and vortex shedding in the separated zone. The possible couplings between these phenomena have to be clarified. Previous experimental studies in compression ramps for Mach numbers of 1.5 and 5 (Dolling & Or 1985; Erengil & Dolling 1991; Thomas *et al.* 1994), proposed some models of interaction between the low-frequency shock motions and the dynamics of the recirculating zone. Generalization of these results in other configurations, for example in the incident shock case, is still an open question, as well as the definition of pertinent length and velocity scales able to normalize the different quantities. For example, Erengil & Dolling (1991*b*) pointed out in a compression ramp experiment that correlations of the dimensionless frequency, or Strouhal number, based on shock motion frequencies could not be deduced directly from subsonic results in detached flows and that the extension of subsonic scaling to supersonic detached flows had to be justified by experiments in various configurations.

The experimental study presented in this paper aims at bringing some insight into the physics controlling such motions together with a detailed study of their unsteadiness for a range of shock intensities. In the following sections, we will present detailed experimental results in a turbulent boundary layer at a Mach number of 2.3 impinged by an oblique shock wave, with flow deflection angles θ varying from 7° to 9.5°. Mean fields have been obtained in the same facility in previous works (Deleuze & Elena 1996; Laurent 1996). Here, we will focus on the unsteadiness related to the shock movements and inside the recirculating flow. Precise descriptions of upstream conditions and the possible presence of low-frequency perturbations due to wind tunnel imperfections and their connection with shock oscillations will be considered. The evolution of the different length and frequency scales will be described along the interaction and at the beginning of the relaxation zone. Then we will propose a compilation of these different results, together with experiments in other geometrical configurations (subsonic detached flows, compression ramp at moderate or high Mach numbers). We will try more particularly to validate whether the initial part of the interaction, the unsteady detached shock and the initial development of the detached zone, can be characterized using generic models, independent of the configuration of the interaction (compression ramp or incident shock) for a wide range of shock intensities. Finally, links between the low-frequency shock motions and the recirculating zone will be addressed for the different cases.

2. Experimental set-up

The experiment was carried out in IUSTI's hypo-turbulent supersonic wind tunnel. It is a continuous facility with a closed-loop circuit; experiments can be performed for typically up to four hours if necessary at a stable operating point with no significant drift of the aerodynamic conditions. The test section is 17 cm wide and 12 cm high. The nominal free-stream Mach number is $M_\infty = 2.3$. The stagnation pressure is kept constant at 0.5×10^5 Pa ± 0.15 % and the stagnation temperature is almost constant around a nominal value of 300 K (typical drift 0.2 K h^{-1}).

A shock generator is made of a sharp-edged plate placed in the free-stream and fixed on the ceiling of the wind tunnel, its leading edge is located in the potential flow. It spans the test section across its whole width and generates an oblique shock wave impinging on the floor boundary layer. Different conditions of SWTBLI are studied by varying the incidence angle of this plate from $\theta = 7°$ to 9.5°. A spark schlieren visualization of the field is shown in figure 1. The visualization shows the incident shock (IS) impinging on the boundary layer (BL) and reflecting from the recirculating zone as an expansion fan. The induced pressure gradient creates, upstream of the IS, a recirculation zone near the wall, which is itself at the origin of the reflected shock (RS) located upstream of the interaction. A detached flow develops over the recirculation zone at a short distance from the foot of the RS and reattaches downstream, with a strong increase of the BL thickness. As the outer stream flows toward the wall there is reattachment and the flow is gradually turned parallel to the wall by weak compression waves. Note that these shocks are very weak and therefore can barely be detected in the schlieren picture.

Spanwise mean static pressure measurements were checked upstream of the interaction over 10 cm (9 boundary-layer thicknesses and 0.6 times the test-section span) and showed good two-dimensionality. However, it is known that mean wall pressure is only a poor indicator of flow three-dimensionality.

Two models were designed to obtain wall pressure fluctuation measurements in the different zones of the interaction. These models are made up of off-centre removable

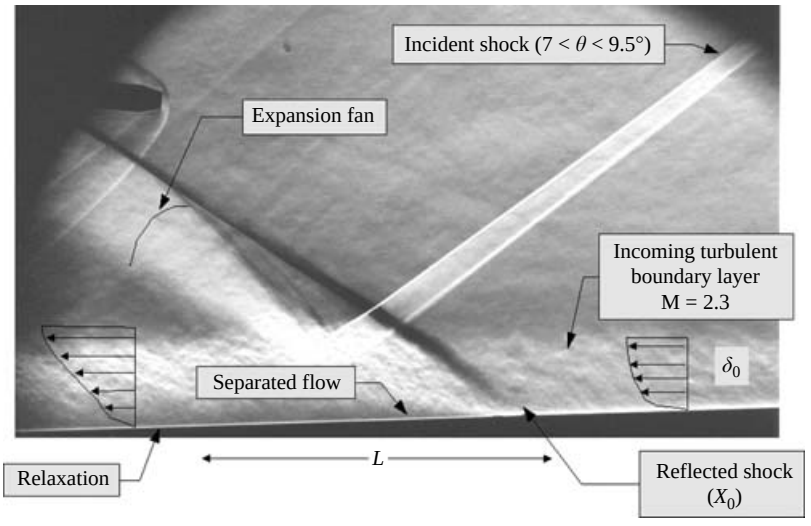

FIGURE 1. Shock reflection with boundary-layer separation – spark schlieren visualization with schematic representation of two-dimensional flow field ($\theta = 8°$).

disks, the smaller one containing three pressure sensors spaced 4.5 mm apart, about half the initial boundary-layer thickness. Any desired location for the transducers can be obtained by rotating the disks over a distance of 13 cm. Thus, the distance between pressure sensors and the incident shock prolongation to the wall varies from $8\delta_0$ upstream to $1.6\delta_0$ downstream.

High-frequency response pressure transducers are used (Kulite series XCW-062). Their pressure range is 0–350 mbars and their bandwidth limit is above 20 kHz. It will be shown that this limit is sufficient to measure the low-frequency unsteadiness of the separated zone. The output of the transducers was amplified via conditioners of bandwidth larger than 100 kHz, and signals were low-passed through filters with cut-off frequencies of 50 kHz. The analogue signals were finally digitized with a sampling frequency of 100 kHz by a Lecroy 6810 A/D converter, and all subsequent data processing was performed on a PC. The spectral processing of wall pressure fluctuations was performed by standard Fourier analysis providing spectra, coherence and phase. Statistical properties (moments, probability density functions, spectral distributions) used 524 288 points. Spectral quantities were obtained by ensemble averaging 64 blocks of 8192 point time series which yields a frequency resolution of $\Delta f = 12$ Hz.

The mass flux fluctuations were measured by a constant temperature hot-wire anemometer (HWA), Dantec Streamline, operating in symmetrical bridge configuration. Probes were made of a tungsten wire of 5 μm in diameter. The aspect ratio of the wires was larger than 200, and the overheat ratio was about 0.6 so that the probe is mainly sensitive to the momentum fluctuation $(\varrho u)'$. The resulting bandwidth is less than 100 kHz in the external flow.

3. Incoming conditions: the upstream boundary layer

The nominal conditions of the interaction are as follows. The incoming boundary layer is turbulent fully developed and has a thickness δ_0 (99 % U_0) of 11 mm, an incompressible momentum thickness of $\theta = 1.28$ mm and a Reynolds number based

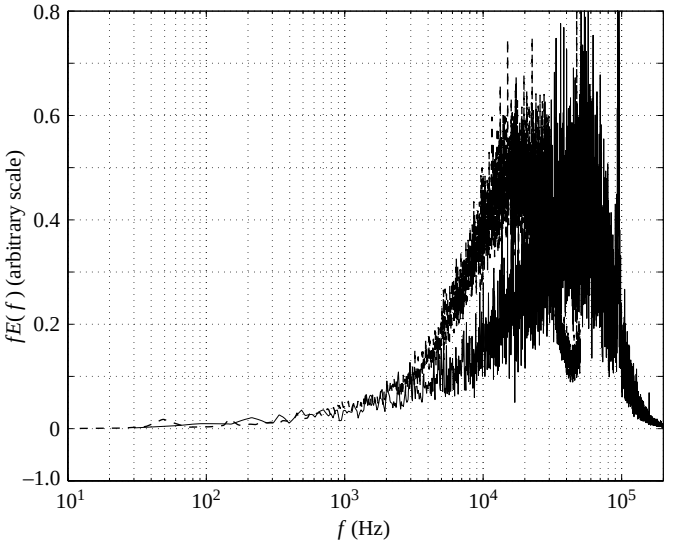

FIGURE 2. Power spectral density in the upstream boundary layer; ——, momentum fluctuations (CTA measurements, $y/\delta = 0.2$), – – –, wall pressure fluctuations, low pass = 50 kHz.

on the momentum thickness $Re_\theta = \rho_0 U_0 \theta/\mu_0$ of 6.9×10^3. In the region with a constant stress τ_w, dimensional analysis leads to the analytical logarithmic law via the Van Driest transformation for the velocity profile $U^+ = (1/\chi)\log y^+ + C$ where $U^+ = \int_0^U (\rho/\rho_w)^{1/2}\,\mathrm{d}u$, $y^+ = yU_\tau/\nu$, where χ and C are constants. The retained values are $\chi = 0.41$ and $C = 5.25$. Adjustment of the friction velocity U_τ provides the best fit of the logarithmic law on velocity data in the range $20 < y^+ < 200$ and determines the skin friction coefficient, $C_f = 2 \times 10^{-3}$.

Laser-Doppler anemometry (LDA) measurements of velocity fluctuations have been carried out by Deleuze (1995) and Deleuze & Elena (1996). The Morkovin's representation takes into account density variation in the scaling of Reynolds stresses and good agreement has been found between supersonic and subsonic flow profiles obtained by Klebanoff (1954).

In Debiève, Dupont & Laurent (2000), measurements carried out in the flow itself by constant current anemometer have provided similar information on spectral properties of the incoming boundary layer: longitudinal velocity, momentum and temperature spectra were measured inside the boundary layer. They showed a maximum of energy for $f\delta/U_0 \approx 0.6$ with a corresponding frequency $f \approx 30$ kHz.

It has been pointed out that low frequencies characteristic of the shock motion are of the order of a few hundred Hz. In order to check if any significant energy in this frequency range occurred in the upstream boundary layer, we have realized measurements of longitudinal mass flux fluctuations with a hot-wire anemometer operating in constant temperature mode (CTA) at $y/\delta = 0.2$. We also performed wall pressure fluctuation measurements with signals low passed to 50 kHz and sampled at 100 kHz in order to describe accurately the low-frequency part of the spectrum. For both quantities, no significant energy was found in the upstream boundary layer in the low-frequency range (see figure 2), so that there is no evidence of low frequencies in the incoming flow produced by peculiarities in the wind tunnel arrangements.

The mean characteristics of the upstream boundary layer are summarized in table 1.

M	U_0	δ_0	Re_θ	C_f	T_t	θ
2.3	550 m s^{-1}	11 mm	6.9×10^3	2×10^{-3}	300 K	1.28 mm

TABLE 1. Aerodynamic parameters of the flow upstream of the interaction.

4. Organization of the interaction

We first give a global overview of the interaction, in order to put in evidence the different zones of the flow where strong unsteadiness are developing. Then, in the following sections, we will characterize more precisely the different time and length scales involved.

The origin of the longitudinal coordinate x is set to the mean position of the reflected shock (X_0) and is normalized by the length of the interaction zone L which corresponds roughly to the distance between the foot of the RS and the reattachment point. It will be defined more precisely in § 5.2 (for example, $L/\delta_0 = 4.18$ for the $\theta = 8.0^\circ$ case). The dimensionless coordinate is therefore $X^* = (x - X_0)/L$. The interaction extends downstream up to $X^* = 1$, which corresponds approximately to the end of the separated bubble. The recirculation zone, characterized by very high levels of fluctuations, extends over the whole interaction zone ($0 < X^* < 1$). Above this region, the mean and turbulent velocity profiles are strongly modified (Deleuze & Elena 1996). The mean velocity profiles have a quasi-linear behaviour in the region $0.1 < y/\delta_0 < 1.2$, and a second maximum of turbulence appears far from the wall (around $y/\delta_0 \approx 0.6$) and is still preseved far downstream of the reattachment point. Following experimental results in subsonic separated flows (Cherry *et al.* 1984; Kiya & Sasaki 1983) this can be interpreted as a mixing layer generated immediately downstream of the mean separation point. This mixing layer constitutes the upper part of the recirculating zone which develops over the counterflow zone and relaxes downstream of the reattachment point. This will be addressed in more detail in § 6.

The longitudinal evolution of the mean value ($\bar{P}$), and the standard deviation (r.m.s.) of the wall pressure $\sqrt{\overline{p'^2}}$ are shown in figures 3 and 4. The dimensionless mean and standard deviation pressure are defined by: $P^* = (\bar{P} - p_1)/(p_2 - p_1)$ and $p'^* = \sqrt{\overline{p'^2}}/(p_2 - p_1)$, where p_1, respectively p_2, are the pressure upstream, respectively downstream, of the incident shock, deduced from the inviscid theory. In the vicinity of the foot of the RS deduced from the schlieren visualizations, a smooth increase of the mean pressure is found. The r.m.s. pressure presents a bump in the same region, with a strong increase in the pressure fluctuations downstream of the RS in respect with the upstream values ($p'_2/p'_1 \approx 9$). The pressure transducers have a cutoff frequency above 20 kHz. Most of the frequencies characterizing the interaction – particularly low frequencies associated with the motion of the reflected shock – are in this frequency range. Of course, turbulent fluctuations in the upstream boundary layer involve much higher frequencies, but the broadband value of the r.m.s. pressure fluctuations is beyond the scope of the present article. Previous wall piezo-electric transducer measurements in the same boundary layer (Debieve 1983; Dolling & Dussauge 1989) already showed that energetic scale frequencies of the BL could be larger than 60 kHz. The evaluation of the level of wall pressure turbulence for the BL based on their measurements provided a r.m.s. pressure value at the wall of 87 Pa, three times higher than that measured in our experiments. This factor 3 shows the

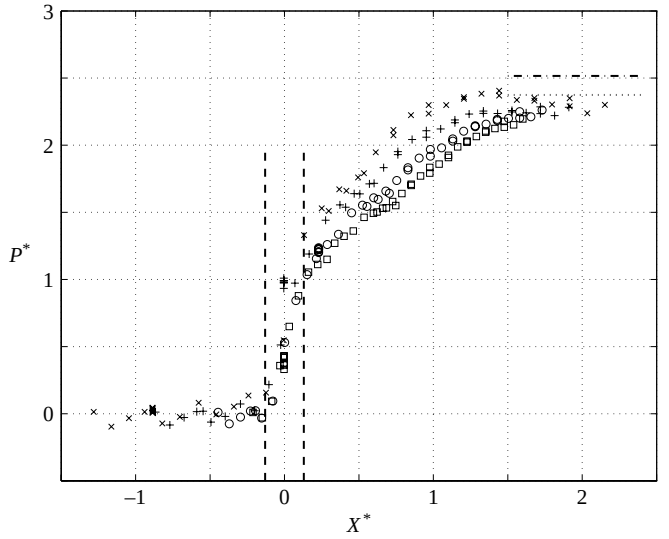

FIGURE 3. $P^* = (\bar{P} - p_1)/p_2 - p_1$ mean pressure distribution along the interaction; ×, $\theta = 7°$; +, $\theta = 8°$; ○, $\theta = 8.8°$; □, $\theta = 9.5°$. Vertical dashed lines delimit the oscillation zone of the unsteady reflected shock; the horizontal dashed lines correspond to the inviscid theoritical values: -.-, $\theta = 9.5°$; . . . , $\theta = 7.0°$.

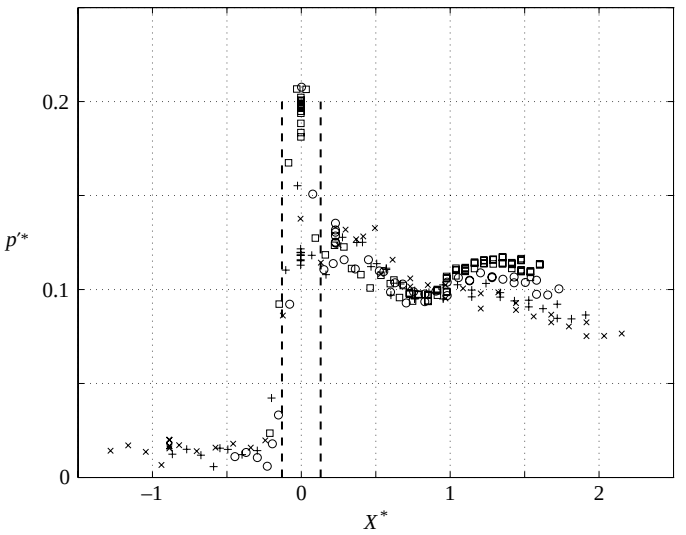

FIGURE 4. Dimensionless r.m.s. wall pressure fluctuations, $p'^* = \sqrt{\overline{p'^2}}/(p_2 - p_1)$, symbols as in figure 3.

underestimation of the r.m.s. due to the cutoff frequency of the pressure transducers used for the present measurements. Thus, the behaviour of this fine-grained turbulence will not be explored in this article which will concentrate on the large time scales developing in the interaction.

The power spectral densities of wall pressure signals have been estimated for positions ranging from the upstream flow to the relaxation, and results for the case $\theta = 8°$ are summarized in figure 5. The chosen representation for spectra is $fE(f)$,

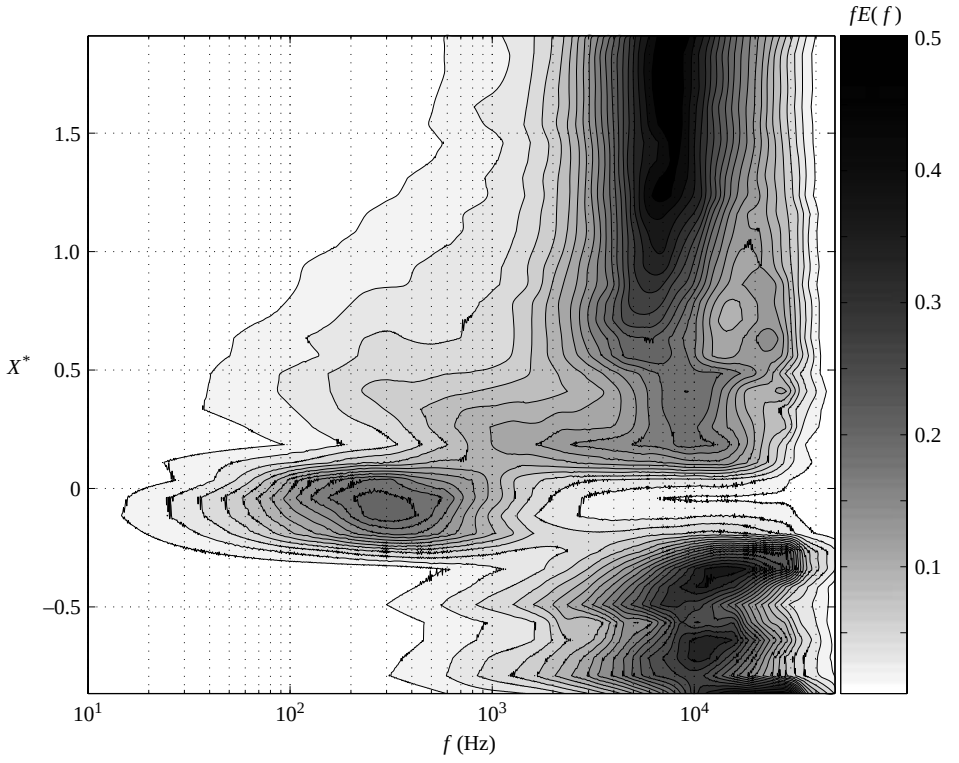

FIGURE 5. Pressure power spectral density along the interaction ($\theta = 8^\circ$).

where E is the PSD normalized to unity. This map shows the frequencies that contribute locally to the energy of the signal. It appears that the frequency ranges are split among four separate zones, each involving characteristic temporal scales:

(i) A high-frequency zone, $X^* < -0.2$, corresponding to the incoming turbulent boundary layer, with energetic frequencies larger than 10 kHz. As mentioned previously, this maximum frequency is strongly underestimated owing to the cutoff frequency of the transducers. Moreover, it should be emphasized that no significant energy was found in the 10 Hz–100 Hz range in the upstream boundary layer.

(ii) The unsteady reflected shock (RS), $-0.15 < X^* < 0.15$ characterized by very low frequencies (some hundreds of Hz). The spatial extent of the foot of the shock motion, L_{ex}, is of the order of $L/3$ or about 1.4 initial boundary-layer thicknesses for the 8° case.

(iii) The interaction zone (IZ), $0.2 < X^* < 1$, is associated with the intermediate scales that develop in the frequency range (1 kHz–10 kHz). These frequencies take place between the low frequencies of the shock motion and the high frequencies associated with the fine-grained turbulence. The maximum frequency presents a longitudinal evolution from $f \approx 10$ kHz at $X^* = 0.2$ to $f \approx 5$ kHz at $X^* = 0.6$). We note that low frequencies ($f < 1$ kHz) are still significant and represent 20 % of the total energy of the signal in this region.

(iv) A relaxation zone (RZ), $X^* > 1$, where the medium frequencies developed inside the IZ are dominant up to sections far downstream of the reattachment point

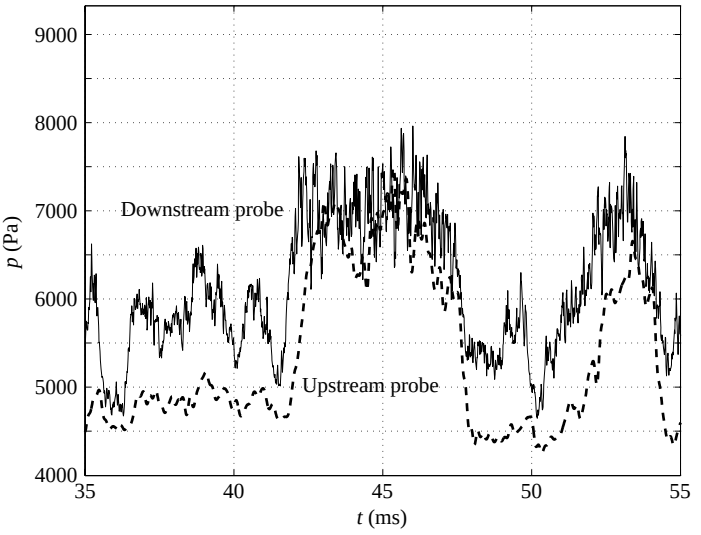

FIGURE 6. Reflected shock pressure signals for two consecutive transducers with a separation distance $\xi = 9.5\,\text{mm}$, $\theta = 9.5°$.

This extends previous results obtained in compression ramp experiments to the incident shock case: the RS is strongly unsteady and moves over distances of the order of magnitude of the initial BL thickness at very low characteristic frequency.

5. Reflected shock: space and time scales

5.1. *Reflected shock pressure signals*

We mentioned in § 4 that the motion of the reflected shock involves large time scales: the PSD exhibits at low frequencies an energy bump without well-identified peaks (see figure 5). To illustrate this behaviour, an example of pressure signals recorded with two transducers in the vicinity of the shock foot is presented in figure 6. The separation distance between transducers is 4.5 mm. The signals show steps due to the low-frequency movements of the RS, with turbulent fluctuations on both sides of the shock front corresponding to the upstream or downstream turbulent flow. The matching of roughly two states leads to a probability density function with overlapping bumps. The signals appear to be nested into each other, which is consistent with an oscillating shock: when the shock moves downstream, it reaches the upstream Kulite first and, when it comes back upstream, the inverse occurs. A simple unsteady shock model is used to determine the characteristic evolutions for the various statistical moments of the signal (mean value, r.m.s., skewness, flatness). Originally, it was proposed in the case of a homogeneous turbulence subjected to an oblique shock (Debiève & Lacharme 1985). The objective was to interpret the hot-wire signals obtained in the vicinity of the unsteady shock. This attempt was made mostly to arrive at the determination of the shock intermittency factor from statistical moments of the signal, without using a conditional analysis of the signals based on step detection. The shock is supposed to have a fixed strength δp and to move randomly around a mean position X_0 over a given space length L_{ex}, with a local intermittency coefficient γ which represents the ratio of time spent downstream of the shock over the total period. The mean pressure upstream of the RS is p_u and downstream p_d,

therefore $\delta p = p_d - p_u$. For the sake of simplicity, the level of turbulence upstream (p'_u) and downstream (p'_d) of the shock is neglected (i.e. $p'_i/\delta P \ll 1$). The various statistical moments of order n of the resulting signal can be written with respect to the intermittency factor and conditioned moments in each state:

$$\overline{p}^n = \gamma \overline{p}_d^n + (1-\gamma)\overline{p}_u^n.$$

This case would be relevant, for example, when applied to measurements made across the shock in the potential flow over the interaction, or for strong shock. The different moments are then given by:

$$n = 1 : (\overline{p} - p_u)/\delta P = \gamma,$$
$$n = 2 : (\overline{p'^2}/\delta P^2) = \gamma(1-\gamma).$$

The normalized mean pressure increases over the length of excursion of the shock, and corresponds to the intermittency factor γ. At the median position of the RS ($\gamma = 1/2$), the normalized r.m.s. value of the pressure fluctuations reaches a maximum and the skewness factor is equal to 0. When the shock reaches its excursion limits (where γ is 1 or 0), the r.m.s. value produced by the shock motion drops to zero. The r.m.s. is an even function with respect to γ with symmetry at $\gamma = 1/2$.

A more elaborate formulation has been derived by taking into account the upstream and the downstream turbulence. To describe the case with additional turbulence, we have to qualify the statistical properties of the upstream and downstream turbulence. We consider a turbulence on both sides of the shock with r.m.s. values equal to the measured values far upstream and downstream of the shock location and supposed independent of the shock motions. The previous relations become:

$$n = 1 : (\overline{p} - p_u)/\delta P = \gamma, \quad \text{unchanged},$$
$$n = 2 : \overline{p'^2}/(\delta P)^2 = \gamma(1-\gamma) + (1-\gamma)(p'_u/\delta p)^2 + \gamma(p'_d/\delta p)^2.$$

Qualitatively, these expressions are very similar to the non-turbulent case, but the symmetry with respect to the median position of the shock disappears as downstream turbulence intensity increases.

As a matter of fact, the model predicts an extremum for the normalized r.m.s. pressure fluctuations of about 0.5 at the median position of the RS. Nevertheless, some difficulties can appear to apply these relations on experimental results. Actually, the pressure p_u and p_d on both sides of the RS can be a function of its position (see figure 6). This behaviour was also pointed out in a compression ramp case (Erengil & Dolling 1991*a*), where the separation shock was followed by compression waves with variable intensity depending on its position. In our case, we used a rough estimate of the pressure jump through the RS (δp) given by the pressure jump through the IS. Such a value strongly underestimates the results given by the previous expressions (see figure 4). Nevertheless, the evolutions predicted by the previous scheme for the statistical moments are similar to the experimental evolutions. So it seems possible to use the statistical moments obtained with pressure transducers at the wall or by a hot-wire anemometer in the field, to determine two space properties of the reflected shock:

(i) Its median position ($\gamma = 1/2$) defined as the location of the maxima of the r.m.s. of pressure signals.

(ii) Its length of excursion (L_{ex}) which is the amplitude of the shock motion around its mean position. This scale is defined as the width of the bump, when the level of r.m.s. pressure equals the maximum reduced by a factor 1/e.

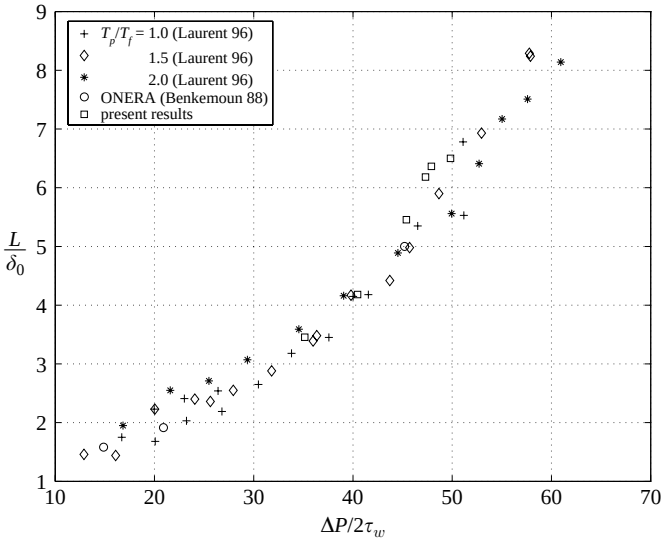

FIGURE 7. Interaction length dependence on the normalized shock intensity.

5.2. *Space and time scales*

A first scale of space is the length of interaction L, defined as the distance between the mean position X_0 of the RS and the extrapolation to the wall of the incident shock wave (X_1). The length L characterizes the upstream displacement of the reflected shock by comparison to the case of perfect flow. As can seen in figure 7, it appears that the interaction length increases with the shock intensity $\Delta p/2\tau_w$, where Δp is the pressure rise across the shock system and τ_w is the wall shear stress upstream of the interaction. In the same figure, we have reported results obtained by Laurent (1996) and Benkemoun & Salaun (1988) in the same configuration, but with a heated wall. In these experiments, the floor of the test section was heated, with a wall temperature T_p ranging from the adiabatic case to twice the recovery temperature T_f of the BL (i.e. $1 < T_p/T_f < 2$). This produces significant variation of the wall friction τ_w independently of the shock intensity. The angle of the shock generator was set from 4° to 8°. For these experiments, the device heating the wall had proscribed the use of unsteady pressure transducers, so no pressure fluctuations were measured, and the length of the interaction was deduced from schlieren visualizations. The set of data ($4 < \theta < 9{,}5°$, $1 < T_p/T_f < 2$, $10 < \Delta P/2\tau_w < 60$) collapses onto a single curve with a monotonic increase of L/δ_0 as the shock parameter $\Delta P/2\tau_w$ increases. Therefore the length of interaction as defined in the present work provides a relevant length scale to characterize the interaction zone. In the case of the strongest shock intensities, when separation occurs, this length can be considered as an estimation of the separation length.

To describe the shock motions, the shock scheme is again used to evaluate the length of displacement of the RS, L_{ex}. To describe the shock movements at the wall, pressure transducers are considered and far from the wall, hot-wire measurements are carried out. The hot-wire probe is located across the local mean position of the RS, deduced in a first step from the schlieren visualizations; two explorations are made at $y/\delta = 1.36$ and 3.45. We obtain a linear increase in the excursion length of the shock with the shock intensity, but it decreases above the boundary layer (see table 2). Then

	$\Theta = 7°$	$\Theta = 8°$	$\Theta = 8.8°$	$\Theta = 9.5°$		
y/δ_0	0	0	0	0	1.36	3.45
$\Delta p/2\tau_w$	35	40.5	45.4		50	
L/δ_0	3.45	4.18	5.45		6.45	
L_{ex}/δ_0	1.17	1.34	1.36	1.68	0.97	0.58
L_{ex}/L	0.34	0.32	0.25	0.26	0.15	0.09
$S_l = f_{sh}L/U_\infty$	0.040	0.035	0.030	0.025	0.025	0.025
U_{RS}/U_∞	3%	2%	1.5%	<1.5 %	<1.5 %	<1.5 %

TABLE 2. Characteristic lengths and frequencies in the interaction.

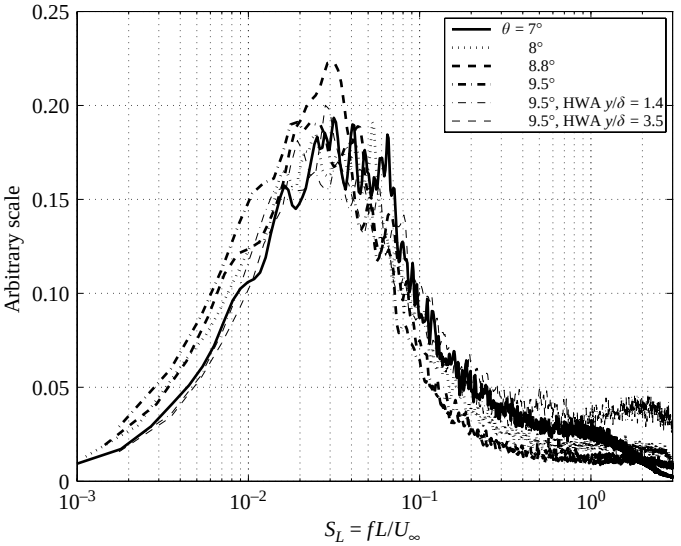

FIGURE 8. Pressure and hot-wire signal power spectral density on the reflected shock ($X^* = 0$).

it is proposed to choose L (or L_{ex}) as a characteristic length scale of the interaction. In order to build a time scale, we must consider also a characteristic velocity. We propose to use the length scale L and the external velocity immediately downstream of the RS, U_∞, to normalize the frequency of the motion of the RS. This leads to a Strouhal number defined as $S_L = fL/U_\infty$. Figure 8 presents the evolution of the PSD deduced from wall pressure measurements near the median position of the RS for the studied set of shock intensities. In the same figure are reported Strouhal numbers obtained in the flow with HWA. It is clear that the same frequency scales are involved, though the amplitude of the reflected shock motion decreases with the distance from the wall. A Strouhal number in the range 0.025–0.04 is obtained for the experimental configurations examined here, including not only variations of distance from the wall, but also variations of shock intensities. The results reported in table 2 show that S_L has a typical value of 0.03 ($\pm 20\,\%$) for the shock intensities considered. To give some insight into the global movements of the shock sheet, hot-wire signals in the flow above the boundary layer ($y/\delta = 1.36$ and 3.45) and wall pressure fluctuations at the mean position of the RS are recorded simultaneously. The coherence function between both signals is defined as: $coh(f) = |S_{12}(f)| / \sqrt{S_{11}(f)S_{22}(f)}$ where S_{12} is the

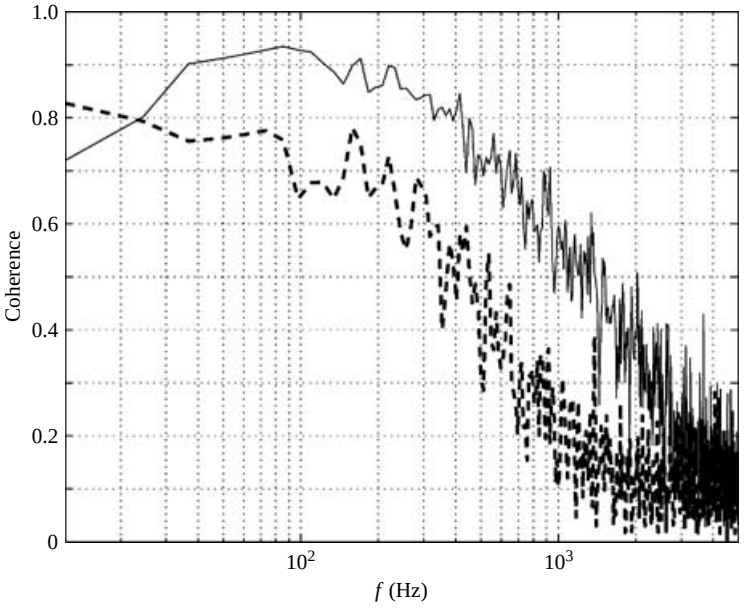

FIGURE 9. Coherence function near the median position of the reflected shock between wall pressure and hot wire signals outside the boundary layer ($\theta = 9.5°$). —, $Y = 15$ mm; – – –, $Y = 38$ mm.

cross spectrum between the two signals and S_{ii} the respective power spectral densities (figure 9). At least at low-frequencies, the movements of the reflected shock at the wall and in the field above the boundary layer are effectively almost in linear dependence, with a high level of the coherence function between the two signals, the average phase lag deduced from the Fourier analysis being essentially zero. Thence, the RS appears as a low-frequency unsteady sheet with a length of excursion vanishing far from the wall and for which one characteristic time scale can be defined. Then, combining time and space scales of the reflected shock, and assuming that the shock moves over $2L_{ex}$ during the time $1/f$, an average velocity U_{RS} for the reflected shock can be derived: $U_{RS}/U_\infty = 2L_{ex}f/U_\infty = 2(L_{ex}/L)S_L$. Table 2 sums up the different values, which were obtained. U_{RS}, in the present experiments, is always less than 3 % of the external velocity. Keeping in mind that this velocity is an average velocity and not the instantaneous velocity, these low values suggest that the reflected shock can be considered as quasi-static, without strong additional dynamic effects, as for example, an emission of additional compression or expansion associated with its acceleration.

6. Interaction zone

This part presents spatial and temporal properties of the fluctuations observed in the IZ. This region is particularly difficult from an experimental point of view because of the presence of recirculating flow, very high turbulence intensities, shocks and an expansion fan. Moreover, a large part of this region is transonic, which means that it is difficult to use hot-wire probes in this part of the flow. Consequently, most of the results will be deduced from wall pressure measurements.

The longitudinal evolution of the PSD of pressure fluctuations was presented in §4 in the case $\theta = 8°$ (figure 5). This revealed new energetic frequencies in the IZ,

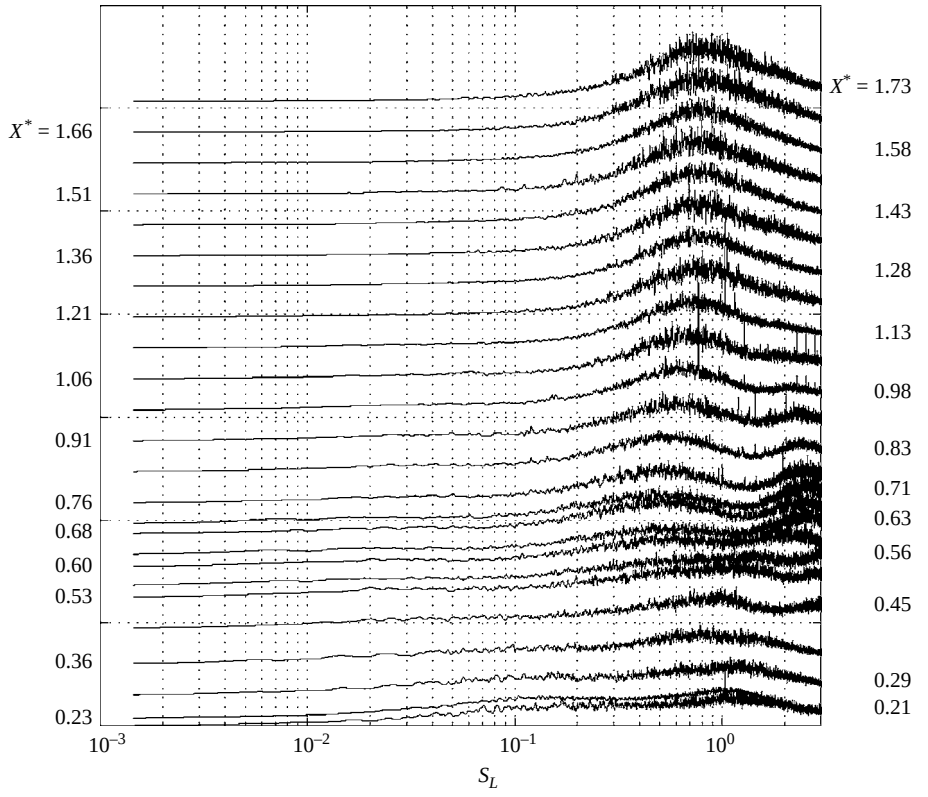

FIGURE 10. Longitudinal evolution of the pressure PSD inside the interaction zone ($\theta = 8.8°$). $0.20 < X^* < 1.73$.

downstream of the reflected shock. Similar results are obtained for the other cases of shock intensity. Section 5.2 has shown that a relevant length scale for normalizing RS motion frequencies is the length of interaction L. We propose to use the same scale for the IZ, i.e. to consider the dimensionless frequency $S_L = fL/U_\infty$. This Strouhal number is similar to that defined in subsonic recirculating flows where the length scale L is the length of separation of the flow (see for example Kiya & Sasaki 1983). We show in figure 10 the longitudinal evolution obtained in the case $\theta = 8.8°$, from the beginning of the interaction up to the relaxation zone. As for $\theta = 8°$, the PSDs, in the $fE(f)$ representation, are found to reach a maximum level in a medium frequency range ($0.3 < S_L < 2$), which varies with X^*. The evolution of these dominant frequencies along the interaction for the different shock intensities under study is summarized in figure 11. Cherry *et al.*'s results obtained in a separation bubble formed along the sides of a blunt flat plate with right-angled corners are also reported in figure 11. A classical interpretation in subsonic recirculating flows is to associate these frequencies with the large convective scales of the mixing layer which develop from the separation point (Kiya & Sasaki 1983; Cherry *et al.* 1984). In such case, the large structures' length scale λ increases linearly as they are convected downstream ($\lambda \propto x$, where $\lambda = U_c/f$, U_c is the convection velocity of the structures and f the associated frequency): this leads to a linear evolution of the inverse of the frequency f, hence S_L^{-1}. Such a behaviour is observed at the beginning of the interaction ($X^* < 0.5$), but is followed by a constant level in the second half of the

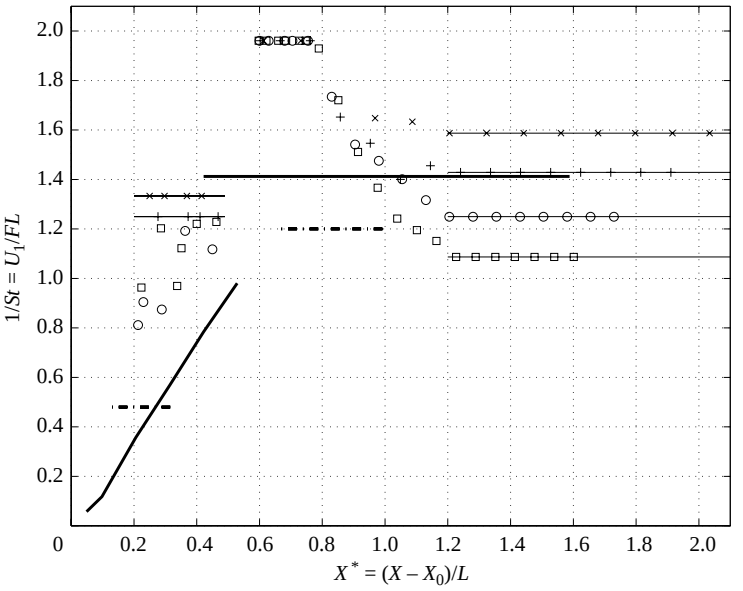

FIGURE 11. Longitudinal evolution of S_L; —, subsonic detached flow Cherry *et al.* (1984); -·-, $M = 1.5$ ramp flow Thomas *et al.* (1994); present experiments ×, $\theta = 7°$; +, $\theta = 8°$; ○, $\theta = 8.8°$; □, $\theta = 9.5°$.

recirculating bubble which is associated with some vortex shedding in the downstream flow. Such a hypothesis still seems relevant in our case (see figure 11). Nevertheless, even if strong similarities are observed, there are important differences. First, for the smallest shock intensities ($\theta = 7°$ and $8°$), the behaviour of the first part ($0 < X^* < 0.5$) is not continuous as in a mixing layer, but the Strouhal number experiences step variations suggesting that it jumps from one initial spatial organization to another at a quite well-defined position ($X^* \approx 0.5$). On the other hand, stronger shock intensities produce continuous evolution of the dominant frequency as in low-speed separations. This would suggest, for shocks of low intensity, some spatial feedback mechanism that synchronizes the merging processes occurring inside the mixing layer. The second part of the IZ ($0.5 < X^* < 0.8$) is similar to subsonic organization, with a nearly constant shedding frequency (around $S_L \approx 0.5$) for the whole range of shock intensities. For all cases, and in a way different from the subsonic scenario, the dimensionless frequency increases continuously in the region $0.8 < X^* < 1.2$, and then reaches a nearly constant value depending on the shock intensity in the beginning of the relaxation.

The kinematics of these scales have been addressed through two-point measurements. Two Kulite transducers have been used with a probe separation $\xi = 4.5\,\mathrm{mm}$. The phase velocity associated with the dominant frequency is defined by $V_\phi = 2\pi f \xi/\phi$, where ϕ is the phase deduced from the cross-spectra, and is presented in figure 12 for the different shock intensities along the IZ. For all cases, in the region $0.2 < X^* < 0.8$, where the spatial evolution of the dominant frequency is similar to the subsonic results, a mean value of approximately $150\,\mathrm{m\,s^{-1}}$ is obtained with a slight decrease near the reattachment point. Then, a strong increase of the phase velocity is observed in the region $0.8 < X^* < 1.2$, where the dominant frequencies have been found to increase. This region starts at the expansion fan associated with the reflection of the incident shock.

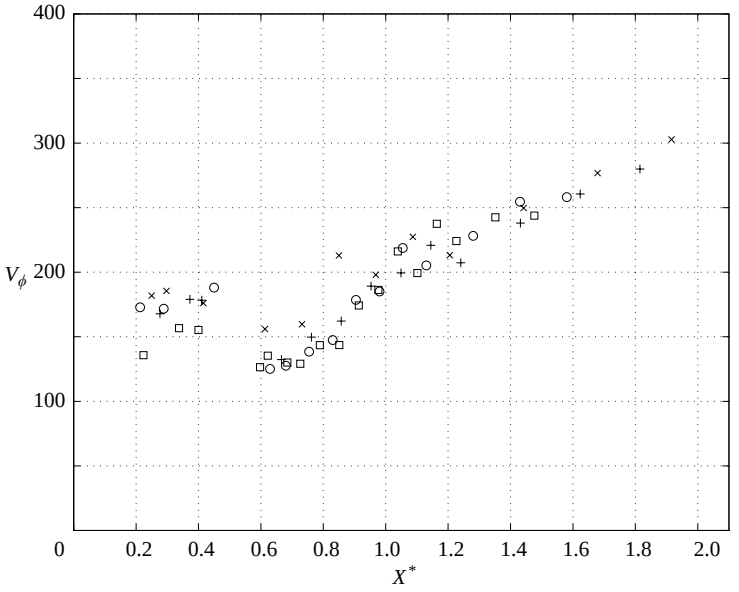

FIGURE 12. Phase velocities ($\mathrm{m\,s^{-1}}$) of the characteristic frequency along the interaction (symbols caption as in figure 11).

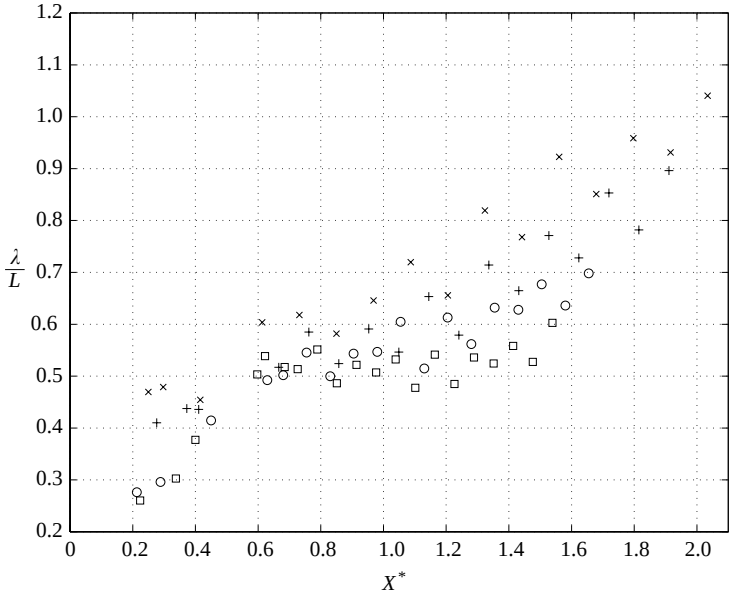

FIGURE 13. Wavelength along the interaction (symbols caption as in figure 11).

Some differences appear also when the structures shed in the relaxation zone are considered. From the Strouhal number and from the associated phase velocity, the wavelengths λ have been estimated from: $\lambda = V_\phi/f$, or $\lambda/L = S_L^{-1} V_\phi/U_\infty$. They are presented in figure 13. Again two families appear: low and high shock intensity. For high shock intensities, structures of approximately half of the interaction length are advected downstream. For low shock intensities, if the original wavelength (at

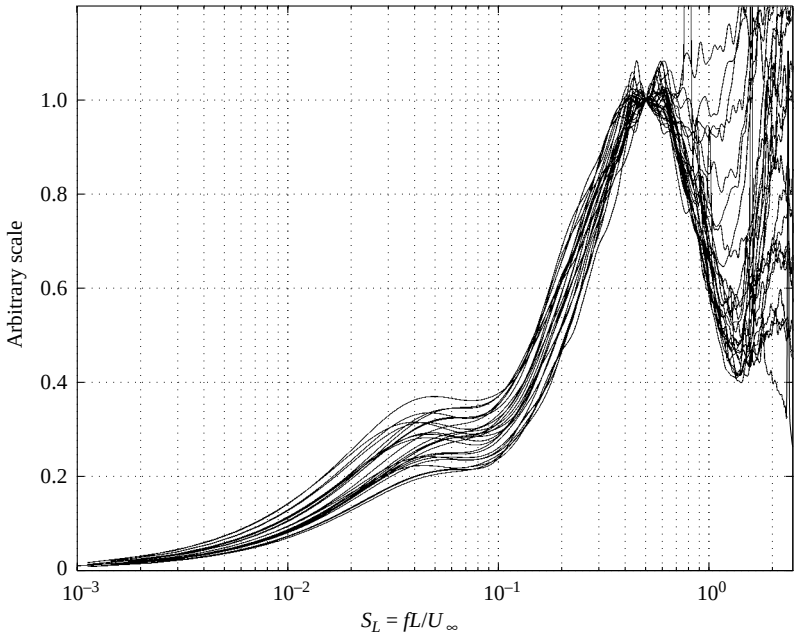

FIGURE 14. Pressure power spectral density inside the interaction zone for the various shock intensities ($7.1 < \theta < 9.5^\circ$ in the region $0.6 < X^* < 0.77$).

$X \approx 0.6$) is about the same, it increases significantly along the flow. Inside the IZ and for all cases, these scales present a large overshoot of coherence ($Coh \approx 0.8$) for the whole set of shock intensities and spatial positions ($0.2 < X^* < 1.4$).

In addition to the frequencies associated with large convected scales over the recirculation ($S_L \approx 0.5$), low frequencies ($S_L \approx 0.04$) with no negligible energy, in the same range as for the RS motions, are observed in the region $0.6 < X^* < 0.8$ (see figure 14). These low frequencies have quasi-null phase shift between sensors, even for probe separations of 9 mm. Therefore, the pressure fluctuations in the IZ have a dispersive behaviour: the intermediate scales ($S_L \approx 0.5$) have been found to be convective with a phase velocity $V_\phi \approx 0.3U_\infty$ when the low frequencies ($S_L \approx 0.04$) correspond to nearly in-phase fluctuations. Moreover, if we consider the coherence function of the low frequencies inside the IZ, a typical linear behaviour is found ($Coh = 1$), even higher than for the intermediate frequencies.

In order to confirm the link between the low frequencies associated with the RS motions and those found in the second part of the IZ, near the reattachment point, wall pressure fluctuations measured at the median position of the RS and near the end of the IZ are recorded simultaneously ($X^* = 0$ and $0.73 < X^* < 1.04$). A strong coherence is found for the low-frequency range (figure 15) with phase shift between signals equal to π (figure 16): the low-frequency fluctuations at the shock foot and close to the reattachment are out of phase.

7. Discussion and conclusions

The results presented in §§4 to 6 give an overview of the interaction for a wide range of shock intensities. As mainly wall pressure measurements have been performed inside the IZ, the structure of the flow is seen from the wall and probably does not

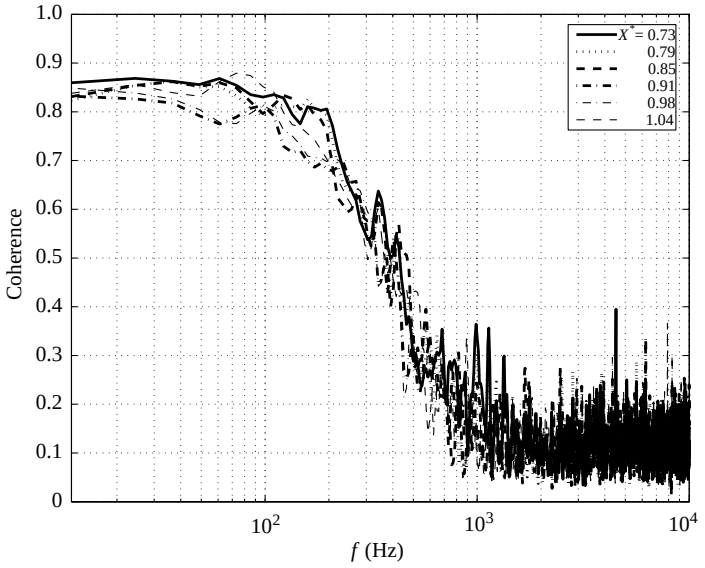

FIGURE 15. Coherence function between wall pressure signals recorded in the vicinity of the reflected shock and near the reattachment region, $\theta = 9.5°$.

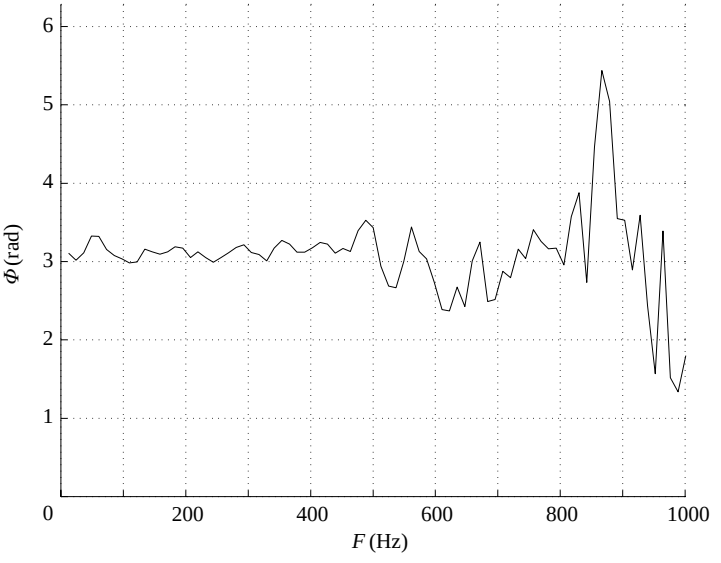

FIGURE 16. Phase shift between pressure signals taken in the vicinity of the reflected shock and the end of the interaction zone, $\theta = 9.5°$. —, $X_1^* = 0$, $X_2^* = 0.98$.

reflect the details of the turbulent structures. However, it is believed that the main features of the interaction are captured in this way. The interaction can be separated into five principal zones, each involving typical temporal scales that extend over two orders of magnitude. These different zones and their principal properties are given below.

1. An adiabatic turbulent boundary layer which is impinged by a steady two-dimensional incident shock. In this incoming flow, no evidence of low frequencies being energetically significant was observed (figure 2).

2. An unsteady reflected shock upstream of the IZ which can be described as a shock sheet oscillating around a mean frequency such as $S_L \approx 0.03$ with a space amplitude of motion increasing linearly with the shock intensity and vanishing far from the wall (figure 8).

3. A mixing layer reattaching near the end of the interaction with large scales developing as in subsonic separations: they are advected downstream (figure 11). In our case, there is a strong acceleration, downstream of the expansion fan ($X^* \approx 0.8$).

4. Superimposed on these scales, frequencies of one order of magnitude lower ($S_L \approx 0.04$) have been identified in the second part of the IZ (figure 14). They contribute up to 30 % of the total energy of the pressure fluctuations and with nearly linear dynamics over a distance of δ_0 (their coherence function is nearly one) with an average phase lag of almost zero. These low frequencies are in the same range as the characteristic frequencies associated with the reflected shock. Their origin is still not well identified, but it can reasonably be expected that they participate significantly in the movements of the RS.

5. A relaxation zone downstream the IZ which develops downstream.

If we consider first the RS unsteadiness, it has to be noted that Erengil & Dolling (1991*a*), in a Mach 5 compression ramp interaction, have found that the characteristic dimensionless frequency for the shock unsteadiness is also close to 0.03. In an $M = 1.5$ compression ramp experiment, Thomas *et al.* (1994) have estimated the average frequency at which the shock crosses the measurement location. If we use half of this frequency as an estimate for the mean frequency of the shock motion, and their estimation of the detached length to evaluate the Strouhal number, a similarly low value is derived: $S_L \approx 0.04$. Then, although the results are somewhat scattered, the different configurations of SWTBLI considered here lead to typical values for the frequency of the shock unsteadiness, which scale reasonably on the size of the interaction and on the external velocity.

This length, which is an estimate of the separation length for the detached cases, has also been retained inside the IZ to compare the different SWTBLI configurations with separated subsonic flows. Nevertheless, if the mixing-layer zone presented some similarities with subsonic detached flows, and the collapse of the data is very efficient in the present experiments (see the vortex shedding frequency on figure 11), the Strouhal numbers were found to be different from the subsonic ones. In a first attempt to understand this behaviour, classical properties of incompressible and compressible mixing layers have been used. We compared the Strouhal number in similar compressible and incompressible (noted 0) recirculating flows, that is, with counterflows of the same velocity and density ratios on both sides of the mixing region. The Strouhal number can be expressed as:

$$S_L = \frac{fL}{U_\infty} = \frac{U_c}{U_\infty}\frac{L}{\delta_\omega}\frac{f\delta_\omega}{U_c} = \frac{U_c}{U_\infty}\frac{L}{\delta' X}S_{tr} \approx \frac{U_c}{U_\infty}\frac{S_{tr}}{\delta'}X^{*-1}. \tag{1}$$

With $S_{tr} = f\delta_\omega/U_c$, $\delta_\omega = \delta' X$, where δ' is the spreading rate which can be expressed as:

$$\delta' = \frac{\delta'_{ref}}{2}\frac{(1-r)(1+\sqrt{s})}{1+r\sqrt{s}}\Phi(M_c), \tag{2}$$

with $r = U_2/U_1$, $s = \varrho_2/\varrho_1$ and $\Phi(M_c)$ a decreasing function of the convective Mach number, based on the convection velocity of the large coherent scales U_c and the external velocities U_1 and U_2, as defined in Papamoschou & Roshko (1988). For subsonic mixing layers, we have $S_{tr} \approx 0.22$ and $\delta'_{ref} \approx 0.16$ (Browand & Troutt 1985)

and the convection velocity is:

$$\frac{U_c}{U_\infty} = \frac{1 + r\sqrt{s}}{1 + \sqrt{s}}. \tag{3}$$

A fit through the subsonic measurements of S_L *vs.* X^* performed by Cherry *et al.* gives $S_L \approx 0.5X^{*-1}$, which corresponds to $r = -0.1$. This means that the back flow is 10 %, which seems acceptable for recirculating flows. We will assume that there is a back flow of the same intensity in our flow. We will evaluate the effects of compressibility on the development of the mixing layer and the corresponding dimensionless frequency S_L in the case $r = -0.1$ and $s = 1$. It is commonly admitted that δ' and S_{tr} are decreasing functions of the convective Mach number M_c, so that their ratio can be expected to be only a weak function of the convective Mach number. Then, as a first approximation, equation (1) suggests that any significant evolution of S_L has to be related to the evolution of the velocity ratio U_c/U_∞. If we accept the isentropic evaluation (Papamoschou & Roshko 1988), this ratio should be only a function of r and s through the same relation as in subsonic flows, (equation (3)). Previous work, however, has shown (Papamoschou 1989; Barre 1994; Barre, Dupont & Dussauge 1997) that when the convective Mach number becomes supersonic, another behaviour is observed: an asymmetrical shear layer is found and the large coherent scales are no longer convected at the isentropic convection velocity, particularly if the flow confinement is important. In our case, the isentropic relation would give $U_c/U_\infty = 0.5$. If we compare this result with the phase velocity presented in the previous section, it is clear that the isentropic model is not applicable to our flow: an experimental value of about 0.3 is obtained. This departure from the isentropic relation leads to an asymmetric behaviour. Indeed, the convective Mach number relative to the high velocity side ($M_{c1} = (U_1 - U_c)/a_1$) is no longer equal to the convective Mach number relative to the low velocity side ($M_{c2} = (U_c - U_2)/a_2$), as proposed by the isentropic model. We obtain two different Mach numbers, $M_{c1} \approx 1.37$ and $M_{c2} \approx 0.57$. The experimental value, $U_c/U_\infty = 0.3$, used in equation (1) gives $S_L \approx 0.34X^{*-1}$, which is consistent with our results (see figure 11).

If no strong departure from the isentropic estimation is expected for lower convective Mach numbers ($M_c < 0.6$) and if comparable amounts of back flow are considered, results resembling the subsonic case are expected. In order to validate this assumption, Thomas *et al.*'s results along the interaction have been considered and are reported in figure 11. They show the same behaviour as in our low shock-intensity cases: two discrete states on both sides of $X^* = 0.5$ are observed. The amount of back flow in this experiment is unknown, but it can reasonably be considered smaller or equal to the amount used in the previous estimations, i.e. 10 % of the external flow. Then, as the convection velocity given by relation (3) is probably correct for this moderate Mach number, the previous scheme suggests that the Strouhal number should be the same as in subsonic flows. Figure 11 shows that, despite the discrete evolution of Strouhal number mentioned above in the first part of the interaction, the shedding frequency measured in this experiment is effectively very similar to its subsonic counterpart. Of course, the typical evolution of the Strouhal number for $0.8 < X^* < 1.2$ of our configuration is not observed in the experiments for the compression ramp where the downstream flow may have very different features.

The present estimations are based on the assumption that expressions for the spreading rate (equation (2)) or convection velocity (equation (3)) are still appropriate for mixing layers with counterflow. This can be expected if the latter is limited. For larger counterflows, some caution must be used, and the accuracy of these relations

is perhaps limited (see Strykowski, Krothapalli & Jendoubi 1996). However, in the cases under examination, this intensity should be moderate, so that this estimate is believed to be reliable. This indicates that again, the velocity scale U_∞ and length scale L used in subsonic detached flows are appropriate for normalizing time scales in supersonic detached flows due to shock interactions, at least in the initial part of the interaction ($0 < X^* < 0.8$) for a wide range of configurations.

To complete the description of the different time scales which are developing inside the IZ, it is recalled that some low-frequency events ($S_L \approx 0.04$), similar to the frequencies of the RS motions, have also been identified in the second part of the IZ. Moreover, these low frequencies are found in quasi-linear dependence with RS motions, with a phase shift of π between the two signals. Such a behaviour has already been found by Thomas *et al.* (1994) in their compression ramp flow. They suggested that the motions of the RS in the upstream (and downstream) direction could be related to some decrease (and increase) of low-frequency fluctuations inside the separated zone. Nevertheless, while the exact mechanism which links both zones has not yet been defined, it seems clear that shock motions at low-frequency which occur in SWTBLI are related to low-frequency events inside the separated zone.

Moreover, the global organization of the interaction seems to separate into two sets: low shock intensities ($\Delta p/2\tau_\omega < 40$) and strong shock intensities. Important modifications in the initial development of the mixing layer as well as in the downstream pressure moments have been pointed out for each set. It is well known that SWTBLI can develop important three-dimensional structures for strong shock intensities which can modify the spatial development of the interaction (Smits & Dussauge 1996). This is probably linked with side effects due to the finite size of the test sections, as well as to the amount of backflow in the recirculating zone. As only wall and hot-wire measurements on the nozzle axis have been performed, this aspect has not been addressed in the present work; this could perhaps explain the strongly three-dimensional structure of the RS observed in schlieren visualizations for the strongest shock intensity. In particular, three-dimensional field measurements with an efficient eduction scheme to analyse large coherent scales are required.

At last, it was possible to define time and length scales to compare efficiently the low-frequency unsteadiness of the detached shock as well as the initial part of the separated zone for such different configurations; however, it appears that the downstream development of large scales depends on the geometrical configuration. In the oblique shock reflection case, a strong acceleration of the structures shed in the layer has been observed downstream of the expansion fan ($0.8 < X^* < 1.2$) associated with the reflection of the incident shock. This cannot be described with the previous length and velocity scales only. For large intensities ($\theta \geqslant 8.8^\circ$), a characteristic wavelength equal to half of the interaction length is identified in the region $0.8 < X^* < 1.5$, despite the strong increase of the convection velocity in this region. In the case of lower shock intensities, the wavelength increases continuously downstream of the location $X^* = 1$. This suggests that the precise organization of the interaction zone must be taken into account and that the scaling of the relaxation zone, which cannot be achieved with only the length and velocity scales of the interaction (U_∞ and L), remains a domain to be investigated.

Part of this work was carried out with the support of the Research Pole ONERA/CNES Aérodynamique des Tuyères et Arrière-Corps (ATAC) and with a grant of the Programme de Recherche Aéronautique sur le Supersonique, monitored by the French Ministry of Research and Technology. Their support is gratefully

acknowledged. Comments of Dr J. P. Dussauge are gratefully acknowledged. Authors are indebted to A. Fouque for his help in processing the data.

REFERENCES

Andreopoulos, J. & Muck, K. C. 1987 Some new aspects of the shock wave–boundary layer interaction in compression ramp flows. *J. Fluid Mech.* **180**, 405–428.

Ardonceau, P., Lee, D. H. & Alziary De Roquefort, T. 1980 Turbulence behaviour in a shock wave/boundary layer interaction. *AGARD CP*-271, Paper 8.

Barre, S. 1994 Estimate of convective velocity in a supersonic turbulent mixing layer. *AIAA J.* **32**, Tech. notes.

Barre, S., Dupont, P. & Dussauge, J. P. 1997 Estimation de la vitesse de convection des structures turbulentes à grande échelle dans les couches de mélange supersonique. *Aerospace Sci. Technol.* **4**, 355–366.

Benkemoun, L. & Salaun, M. 1988 Développement d'une couche limite turbulente supersonique sur une paroi chauffée. Propriétés du champ tubulent et exploitation théorique. *Rapport ONERA* 74/7078.

Beresh, S. J., Clemens, N. T. & Dolling, D. S. 2002 Relationship between upstream turbulent boundary layer velocity fluctuations and separation shock unsteadiness. *AIAA J.* **40**, 2412–2422.

Browand, F. K. & Troutt, T. R. 1985 The turbulent mixing layer: geometry of large vortices. *J. Fluid Mech.* **158**, 489–509.

Chapman, D. R., Kuehn, D. M. & Larson, H. K. 1957 Investigation of separated flow in supersonic and subsonic streams with emphasis of the effect of transition. *NACA TN* 3869.

Cherry, N. J., Hillier, R. & Latour, M. E. M. 1984 Unsteady measurements in a separated and reattaching flow. *J. Fluid Mech.* **144**, 13–46.

Debiève, J. F. 1983 Etude d'une interaction turbulence–onde de choc. Université d'Aix-Marseille, Thèse d'Etat.

Debiève, J. F. & Lacharme, J. P. 1985 A shock wave/free turbulence interaction,. *IUTAM Symp. on Turbulent Shear-Layer/Shock-Wave Interaction, Palaiseau, France, September 9–12, 1985.*

Debiève, J. F., Dupont, P. & Laurent, H. 2000 Compressibility and structure of turbulence in supersonic shear flows. *Eur. J. Mech. B/Fluids* **19**, 597–614.

Delery, J. & Marvin, J. G. 1986 Shock wave–boundary layer interactions. *AGARDograph* 280, NATO.

Deleuze, J. 1995 Structure d'une couche limite tutbulente soumise à une onde de choc incidente. Université de la Méditerranée, Aix-Marseille II, Thèse de Doctorat.

Deleuze, J. & Elena, M. 1996 Some turbulence characteristics downstream a shock wave-boundary layer interaction. *Proc. of the 6th European Turbulent Conference, Lausanne, July 1996.*

Dolling, D. S. 2001 Fifty years of shock-wave/boundary-layer interaction research: what next. *AIAA J.* **39**, 1517–1531.

Dolling, D. S. & Brusniak, L. 1989 Separation shock motion in fin, cylinder, and compression ramp-induced turbulent interactions. *AIAA J.* **27**, 734–742.

Dolling, D. S. & Dussauge, J. P. 1989 Fluctuating wall-pressure measurements. A survey of measurements and measuring techniques in rapidly distorted compressible turbulent boundary layers. AGARDograph 315, NATO.

Dolling, D. S. & Murphy, M. T. 1983 Unsteadiness of the separation shock wave structure in a supersonic compression ramp flowfield. *AIAA J.* **21**, 1628–1634.

Dolling, D. S. & Or, C. T. 1985 Unsteadiness of the shock wave structure in attached and separated compression ramp flows. *Exps. Fluids* **3**, 24–32.

Dupont, P., Debieve, J. F., Ardissone, J. P. & Haddad, C. 2003 Some time properties in shock boundary layer interaction. *Proc. of West East High Speed Flows, January 2003.*

Dupont, P., Haddad, C., Dussauge, J. P. & Debiève, J. F. 2004 Three-dimensional organization and unsteadiness of shock wave/turbulent boundary layer interaction. *Intl Symp. on Interdisciplinary Shock, March 2004.*

Erengil, M. E. & Dolling, D. S. 1991*a* Unsteady wave structure near separation in a Mach 5 compression ramp interaction. *AIAA J.* **29**, 728–735.

Erengil, M. E. & Dolling, D. S. 1991*b* Correlation of separation shock motion with pressure fluctuations in the incoming boundary layer. *AIAA J.* **29**, 1868–1877.

Garnier, E. & Sagaut, P. 2002 Large eddy simulation of shock/boundary layer interaction. *AIAA J.* **40**, 1935–1944.

Green, J. E. 1970 Reflexion of an oblique shock wave by a turbulent boundary layer. *J. Fluid Mech.* **40**, 81–95.

Hakkinen, R. J., Greber, I. & Trilling, L. 1959 The interaction of an oblique shock wave with a laminar boundary layer. *NASA Mem.* 2-18-59W.

Kiya, M. & Sasaki, K. 1983 Unsteady wave structure near separation in a Mach 5 compression ramp interaction. *J. Fluid Mech.* **137**, 83–113.

Klebanoff, P. S. 1954 Characteristics of turbulence in a boundary layer with zero pressure gradient. *NACA TN* 1378.

Laurent, H. 1996 Turbulence d'une interaction onde de choc-couche limite sur paroi plane adiabatique ou chauffée. Universitéd'Aix-Marseille II, Thèse de 3ème cycle.

Lee, B. H. K. 2001 Self sustained oscillations on airfoils at transonic speeds. *Prog. Aerospace Sci.* **37**, 147–196.

Papamoschou, D. 1989 Structure of the compressible turbulent shear layer. *AIAA Paper* 89-0126.

Papamoschou, D. & Roshko, A. 1988 The compressible turbulent shear layer: an experimental study. *J. Fluid Mech.* **197**, 453–477.

Plotkin, K. J. 1975 Shock wave oscillation driven by turbulent boundary layer fluctuations. *AIAA J.* **13**, 1036–1040.

Settles, G., Vas, I. E. & Bogdonoff, S. M. 1976 Details of a shock-separated turbulent boundary layer at a compression corner. *AIAA J.* **14**, 1709–1715.

Smits, A. J. & Dussauge, J. P. 1996 Turbulent shear layers in supersonic flow. AIP Press.

Strykowski, P. J., Krothapalli, A. & Jendoubi, S. 1996 The effect of counterflow on the development of compressible shear layers. *J. Fluid Mech.* **308**, 63–96.

Thomas, F. O., Putman, C. M. & Chu, H. C. 1994 On the mechanism of unsteady shock oscillation in shock wave/turbulent boundary layer interaction. *Exps. Fluids* **18**, 69–81.